Current Chemistry Letters 15 (2026) 369–386

Contents lists available at GrowingScience

Current Chemistry Letters

homepage: www.GrowingScience.com

Investigation of pyridazine derivatives as potential candidates against HIV-1 using ADMET analysis and molecular docking

Mohamed Sahrane[a], Tarik Boutadghart[a], Ikram Mennas[b*], Ahmed Arif[b], Mohammed El idrissi[b*] and Rachida Ghailane[a]

[a]*Laboratory of Organic Chemistry, Catalysis and Environment. Faculty of Sciences. University Ibn Tofail. Kenitra, Morocco*
[b]*Team of Chemical Processes and Applied Materials, Sultan Moulay Slimane University, Polydisciplinary Faculty, Beni Mellal, 23000, Morocco*

C H R O N I C L E

Article history:
Received June 2, 2025
Received in revised form
June 27, 2025
Accepted January 2, 2026
Available online
January 2, 2026

Keywords:
Pyridazine
Reactivity indices
CDFT
HIV-1
Molecular docking
ADMET

A B S T R A C T

The reactions between 2,3-dimethylbutadiene and six azodicarbonyl derivatives give the aromatic α-amino ketone family which presents a great interest in chemical synthesis and especially in polymerization reactions. This reaction was studied using the Molecular Electron Density Theory. The reaction pathways were established using the Intrinsic Reaction Coordinate (IRC) method and confirmed through topological analysis of the Electron Localization Function (ELF). The substituent effect was discussed from the CDFT and GEDT calculations. The temporary formation of hydrogen bonds at TSs is responsible for the mechanistic aspect and the process asynchronous of new bond formation. Consequently, the reaction proceeds via a non-concerted in two-stages mechanism. Finally, we investigated the potential inhibitory effects of six products against HIV-1-Mpro through molecular docking calculations. Then, their medicinal potential and physicochemical properties were scrutinized, employing the SwissADME server, unveiling their non-toxic characteristics and positioning them as promising contenders for drug development.

© 2026 by the authors; licensee Growing Science, Canada.

1. Introduction

Organic reactions using different synthesis methods are only relevant if they are less expensive and produce honorable products that are effectively applicable in several fields. Indeed, the Diels-Alder (DA) reaction is of remarkable importance in organic synthesis, because it provides access to a variety of cyclic and heterocyclic compounds. [1-3] These products possess biological activities and also find their application in industrial uses. This research axe has led to a boom of the development of new methods to improve the yields and all types of selectivity as stereo-/regioselectivity and enantioselective involved in the case cycloaddition reactions. [4-6]

An in-depth theoretical analysis of Diels-Alder reactions, based on the Molecular Electron Density Theory (MEDT) developed by Domingo, [7] offers a different view to that of Molecular Frontier Orbital (FMO) theory, which classically assumes a concerted one-step mechanism involving a single transition state. [4,5] Indeed, the introduction of the concept of conceptual DFT (CDFT)[6,8] where one combines of several parameters and thermodynamic quantities such as indices of electrophilicity [5,9] and nucleophilicity. [10,11] Thus, the analysis of the global electron density transfer (GEDT) taking place at the level of the transition state structure (TS), and of the activation barriers has become a relevant tool for classifying the DA reactions have been classified as non-polar (H-DA), polar (P-DA) and ionic (I-DA) reactions. [9–14]

The DA reactions can take place via one-step or stepwise mechanism depending on if the formation of the two new single bonds occur in one or two steps. This can proceed along several reaction pathways; molecular, radical, zwitterionic, or ionic, [12,15–20] The structural and electronic properties of the diene (D_n) and dienophile (D_p) dictate the reaction profile followed by the reaction, the symmetry of the substrates also implicates the reaction mechanism, and stereo-/regioselectivity of the reaction, which will be less important by comparison in the case where at least one of the reactants is asymmetric.

* Corresponding author
E-mail address ikrammennas321@gmail.com (I. Mennas) m.elidrissi2018@gmail.com (M. El idrissi)
© 2026 by the authors; licensee Growing Science, Canada
doi: 10.5267/j.ccl.2026.1.001

The α-aminoketone derivatives which result from this symmetrical hetero Diels-Alder (SHDA) encompass reagents which give them the characteristics of the aza-Diels-Alder and oxo-DA reactions. Nevertheless, the synthesis of α-aminoketone derivatives via a hetero Diels-Alder (HDA) reaction involves several key steps: diacylhydrazine is oxidized by tert-butyl hypochlorite in the presence of pyridine to yield an azodicarbonyl compound, which is not isolated. The in situ formed azodicarbonyl compound undergoes an HDA reaction with a diene, catalyzed by $Hf(OTf)_4$ or AgOTf, proceeding quantitatively with one equivalent of the diene. α-Aminocarbonyl compounds are essential intermediates in organic synthesis for forming nitrogen-containing molecules. Traditional methods include the oxidation of α-aminoalcohol derivatives and aldol reactions using azodicarbonyl compounds, often resulting in the loss of one nitrogen atom. However, the HDA reaction of thermally unstable azodicarbonyl 1a with 2,3-dimethylbutadiene was challenging due to the easier oxidation of the diene compared to diacylhydrazine, preventing the formation of the HDA product. This synthetic route offers a novel and efficient method for preparing α-aminoketone derivatives. [19-23]

The α-azodicarbonyl derivatives possess high thermal stability, and can be successfully used in polymer synthesis, which is an area of considerable research interest. However, these polymers could also be applied as biological, pharmaceutical, antiviral and agrochemical agents. [24-27]

Such activities are primarily associated with the presence of heterocyclic nitrogen atoms, which play a key role in modulating their interaction with biological systems. [28-30]

In our study, a HDA reaction including N=N active sites of the dienophile will react with carbon sites of the diene (**Scheme** 1). We have also been interested on the substituents effect on the energetic profile. The dienophile has an aromatic ring where the mesomeric and inductive conjugation promotes the effects of substituents which are still important despite their far positions. Herein, the aromatic ring has been substituted in the para position by an electron-donating (ED) or electron-withdrawing (EW) group. Indeed, azodicarbonyl derivatives are used in polymers synthesis which is a research area of considerable interest. [23,24] However, the synthesized polymers could also be useful as biological, pharmaceutical, antiviral, and nutritional agents. [24-27]

MEDT was used to classify these HDA reactions as forward electron density flux (FEDF) and reverse electron density flux (REDF), depending on the direction of the electron density flux at the transition state structure (TS), calculating the reactivity descriptors deriving from the conceptual density functional theory (CDFT) to discuss the effect of the electron-donating (ED) and electron-withdrawing (EW) character substituents on the electronic behaviour of the active sites, The geometric parameters and electronic structures of the transition states were also analyzed based on the results from the NBO calculations. [25,26] The effect of the solvent was taken into account using the polarizable continuum model (PCM) with dichloromethane having a dielectric constant of ε=8.93. [27,31,32]

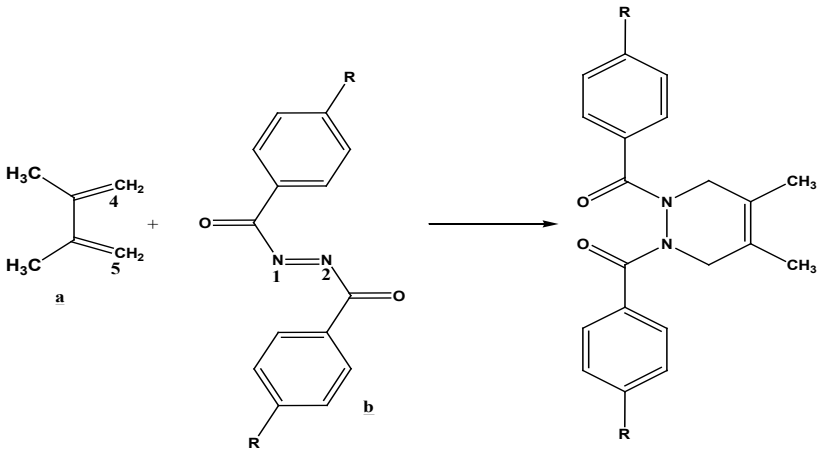

Scheme 1. Hetero Diels-Alder reaction between the 2,3-dimethylbutadiene and azodicarbonyl.

Multiwfn software, [33] based on the monodeterminant wavefunctions of the structures selected along the IRC path, was used to study the evolution of the Electron Localization Function (ELF) [34,35] along the cycloaddition reaction coordinate.

2. Computational Methods

2.1. Quantum chemical

Density functional theory (DFT) provides relevant theoretical information on chemical reactivity and regio/stereoselectivity. Therefore, the Gaussian 09 software has carried out the MEDT computations. However, the B3LYP/6-311G (d, p) technique was used to fully optimize the geometry of transition structures, products, the stationary points, and reactants. In order to guarantee that each transition state (TS) has a single imaginary frequency and that each

minima have zero imaginary frequency, the transition states were described using frequency calculations at 298.15 K and 1.0 atm. Subsequently to verify the energy profiles connecting each transition state to its corresponding reactant and product minima within the proposed mechanism, Intrinsic Reaction Coordinate (IRC) analyses were performed. In addition, the Natural Bond Orbital (NBO) method was used to analyze the electronic structures of the stationary points, as well as the Wiberg bond indices. Furthermore, local and global reactivity analyses were carried out based on the Parr function, employing Natural Population Analysis (NPA). [36] Explaining the reactivity of molecular systems relies on various chemical concepts such as electronic chemical potential μ, global electrophilicity ω, chemical hardness η, and global nucleophilicity N. [10] The calculated values for these descriptors were derived using the following set of equations:

$$\boldsymbol{\mu} = \frac{-(\boldsymbol{I} + \boldsymbol{E})}{\mathbf{2}} \tag{1}$$

$$\omega = \frac{\boldsymbol{\mu 2}}{\mathbf{2}\eta} \tag{2}$$

$$\boldsymbol{\eta} = \left(\frac{\boldsymbol{I} - \boldsymbol{A}}{\mathbf{2}}\right) \tag{3}$$

The global nucleophilicity index N is established with reference to tetracyanoethylene (TCE), which is characterized by low HOMO energy and high electrophilicity. It is determined using the following equation: [6]

$$\boldsymbol{N = E_{HOMO}(nucl) - E_{HOMO}(TCE)} \tag{4}$$

Parr function P(r), which is obtained from the atomic spin density (ASD) is calculated using Eq. (5) for electrophilic attacks and Eq. (6) for nucleophilic attacks.

$$\mathbf{P_k^-} = \boldsymbol{\rho_s^{rc}(k)} \tag{5}$$

$$\mathbf{P_k^+} = \boldsymbol{\rho_s^{ra}(k)} \tag{6}$$

The corresponding local reactive indices (ω_k and N_k) were obtained by the following equations

$$\boldsymbol{\omega_k = \omega P_k^+} \tag{7}$$

$$\boldsymbol{N_k = N P_k^-} \tag{8}$$

The indices of s development (*l*) during a cycloaddition reaction provide information on the process of formation of new bonds, they are evaluated by the following relationship: [37,38]

$$\boldsymbol{l_{x-y} = 1 - \frac{r_{x-y}^{TS} - r_{x-y}^{P}}{r_{x-y}^{P}}} \tag{9}$$

where r_{x-y}^{P} refers to the equivalent interatomic distance in the corresponding product and r_{x-y}^{TS} is the interatomic distance between Y and X in the transition state configuration.

For spin-polarized systems, an ELF study is essential to determine the level of relative electron localization. A large ELF coefficient signals strong electron localization, meaning that there is covalent orbital overlap, involved inner layers of the atom or an isolated pair. ELF analysis has found wide application in various systems, like inorganic and organic molecules, coordination compounds, atomic crystals, and aggregates. Consequently, for the study of aromaticity, the verification of bonding by charge displacement and the classification of chemical bonds. Indeed, we have exploited this computational topology in order to clarify the new bonds mechanism throughout the IRC paths and establish a structural and electronic study of our chemical systems. In our calculations, we used a multifunctional program for the wave function Multiwfn. [31]

2.2. Molecular Docking details

In the docking section, substantial progress has been achieved in developing computational and bioinformatics tools to predict the molecular interactions between a protein and a ligand at the binding site. These advancements are essential for drug design and discovery. The bioinformatics software utilized in this research focuses on molecular reverse docking. [39] The three-dimensional (3D) molecular structures of the pyridazine derivatives were optimized for energy and geometry using Gaussian 09 software with the GaussView 05 interface.The HIV-1 protease crystal structure (PDB identification: 4DJO) was prepared using Discovery Studio by clearing out water molecules and adding polar hydrogens along with Kollman charges. The processed structures were then saved in PDB format. Molecular docking was carried out using AutoDock Vina to assess the binding affinity between each ligand and the target protein. [40] PDBQT files for both the receptor and ligands were generated using AutoDock Tools 1.5.4 from MGL Tools to define the binding site. The docking grid was centered at coordinates x = 20.315, y = 28.231, and z = 18.135, and extended to 40 Å in each dimension with a

spacing of 0.375 Å to allow sufficient flexibility during ligand binding. Interactions between the ligands and active site residues were analyzed using PyMOL [41] and BIOVIA Discovery Studio 2016[42]

2.3. ADMET study

One of the most critical aspects of the drug discovery and development process is the evaluation of the absorption, distribution, metabolism, excretion and toxicity (ADMET) properties of compounds. [43] ADMET studies help scientists determine the suitability of compounds for drug development. We evaluated the pharmacokinetic and physicochemical properties of our six compounds using the SwissADME server and pkCSM. [44] The chemical structures of the designed compounds were converted into SMILES notation after being generated using the SwissADME (build) tool. [45]

3. Results and discussion

3.1. Analysis based on reactivity indices

3.1.1. Global reactivity indices

Several studies conducted on (DA) reactions show that the reactivity indices established by Domingo derived from the conceptual density functional theory (CDFT) [7,46] serve as efficient parameters for evaluating the polar character of such reactions. [9,47] The values of the global reactivity descriptors are shown for all the structures of Schema1 in **Table** 1. Chemical hardness (η) signifies the resistance of ions/atoms/molecules to deformation under weak perturbation during a chemical reaction and fundamentally explains the structural polarization of the electron cloud, chemical softness (S) is defined as the ability of a molecule or atom to receive electrons and presents the reciprocal of chemical hardness, and chemical potential (μ) which provides information about charge transfer between reacting molecules. Thus, the electronic chemical potential for the six dienophiles is between 3.89 eV and 5.32 eV is higher than that of the diene which is worth 3.59 eV. Therefore, the GEDT will be from the diene to the dienophile, it is indeed a FEDF. Furthermore, the values of (ω, N) relative to the dienophiles and the diene indicate that the dienophiles will act as a strong electrophile and the diene behaves as a strong nucleophile. To verify the (NED) character of the different reactions (SHDA) we will then calculate the charge transfer between the two fragments in the interaction of different transition structures.

Table 1. Electronic chemical potential (μ), global electrophilicity (ω), chemical hardness (η), and global nucleophilicity (N) (in eV).

	μ	η	N	ω
a	3.59	5.57	2.98	1.16
b1	4.52	4.07	-6.56	2.51
b2	4.85	3.97	-6.84	2.95
b3	4.37	4.10	-6.42	2.33
b4	4.30	4.11	-6.35	2.24
b5	3.89	4.15	-5.97	1.82
b6	5.32	3.84	-7.24	3.68

3.1.2. Local reactivity indices

The various studies of the regioselectivity of the DA reaction and Hetero DA reaction (HAD) have shown that the analysis of the local electrophily ω_K in the electrophile and the local nucleophily N_k in the nucleophile makes it possible to predict the regioselectivity in the pathway's competitive reactions of this type. Bearing, for our reactions, the interest is to analyze the effect of the substituents for the different substituted dienophiles, since the two fragments involved in our reactions are symmetrical. Therefore, the electrophilic power of nitrogen atoms reacts as electrophilic sites increases with the inductive and mesomeric effect of the substituents knowing that the latter prevails. In addition, the aromaticity and the carbonyl (-C=O) which is attached directly to the active sites further promote the delocalization of π electrons. Analysis of the local electrophilicity indices ω_k, which are 0.45 and 0.38 eV for dienophiles b2 and b6 respectively, are higher than those associated with dienophiles b3, b4 and b5, whose values range from 0.30 to 0.34 eV (**Table** 2). This result is in good agreement with the nature of the Cl and CN substituents carried by b2 and b6 respectively, which exhibit a greater electron-withdrawing effect than the CH_3, OH and NH_2 groups substituting the b5, b4 and b3 dienophiles.

Table 2. Local indices nucleophilic N_K and electrophilic ω_k(in eV).

	a	**b1**	**b2**	**b3**	**b4**	**b5**	**b6**
	C5/C4	**N1/N2**	**N1/N2**	**N1/N2**	**N1/N2**	**N1/N2**	**N1/N2**
$\omega_{(K)}$	0.50	0.39	0.45	0.34	0.34	0.30	0.38
$N_{(k)}$	1.45	-1.55	-1.26	-1.34	-1.15	-0.47	-1.53

3.2. Mechanistic study, geometries and charge transfer at TSs

The analysis of the results indicates that these SHDA reactions take place according to concerted asynchronous processes, such that the different transition state structure (TS) and their associated corresponding products are located and characterized with the total and relative energies cited in **Table** S1 and the reaction profile is shown in **Fig**. 1, as well as the Geometries of the different transition state structure (TS) are illustrated in **Fig**. 2. The structures of the transition states are identified thanks to the analysis of the vibrational frequency. Indeed, each transition state is characterized by a single imaginary frequency.

3.2.1. Mechanistic study

According to the values given in the additional file 1: **Table** S1, the activation enthalpies and the activation Gibbs free energies are positive and range from 20.70 to 26.23 Kcal/mol and from 34.51 to 41.41 kcal/mol respectively. Indeed, the enthalpy and free enthalpy values for all reactions are negative. This means that all reaction paths are thermodynamically possible, since compound formation follows an exothermic process. Furthermore, the entropy variation between reactants and products is negative, with a value of less than -47.92 Cal/mol.K for the different reaction paths, so all chemical systems are evolving towards more ordered states.

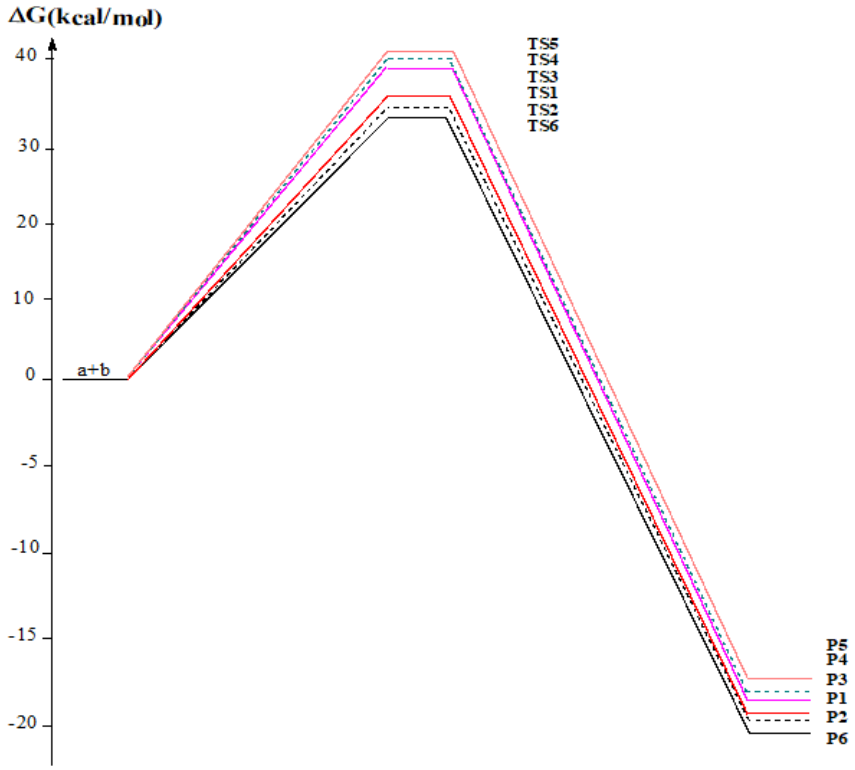

Fig. 1. Diagram of Gibbs Free Energy ΔG (in kcal/mol) of transition structures and products of six studied reactions in the presence of solvent (CH_2Cl_2).

Obtaining a product from a reaction profile depends not only on its thermodynamic stability in relation to the reactants, but also on the rate of formation deduced from the study of chemical kinetics. In this study, among the six α-aminoketone derivatives obtained, we deduce that the most thermodynamically stable product is favored kinetically. For the two products substituted with Cl and CN groups, the most favorable reaction path is obtained with a low activation barrier estimated at 35.67and 33.38 kcal/mol, these products are the most thermodynamically stable with a free enthalpy variation ΔG estimated at -22.23 and -23.55 kcal/mol. The products obtained from dienophiles substituted with CH_3, OH and NH_2 groups are less stable than the unsubstituted product, with instability ranging from -0.07 to -2.63 kcal/mol. On the other hand, groups with a greater mesomeric effect favor the delocalization of π electrons. As a result, the electrophilicity of active sites increases, maintaining interactions between nitrogen atoms and carbon atoms leading to the formation of the most stable cycloadduct, depending on the nature of the substituents.

The results presented in the additional file 1: **Table** S2 and the energy profiles illustrated in **Fig**. S1 show that in the presence of solvent, the activation energy barriers of the six reactions were not significantly modified, resulting in a slight influence on the chemical kinetics of the reaction with a difference of approximately 2 to 5 kcal/mol. This variation is due to the polarity of the solvent, which induces an electric field. The energy profiles of the reaction pathways plotted from the

energy values determined in the condensed phase of the six cycloadditions studied show that the stability of the products is affected in the presence of Dichloromethane.

3.2.2. Geometry analysis of TSs, transition vectors and frequency analysis

The optimized the transition state (TS) geometries corresponding to the six reactions are shown in **Fig**. 2 and the development indices associated with the same links for the six-transition state structure (TS) are reported in **Table** 3. The obtained results clearly show the influence of the existence of the hydrogen bond in the transition state structure (TS) is very remarkable and it causes a temporal asymmetry which reflects the synchronicity of the formation of new bonds, such as the stage of advancement of the single-bond C_5-N_2 located next to of the carbonyl interrogated in the hydrogen bond is more important, it varies between the values (l=0.70 and l=0.76) compared to that which is low values integrating from l=11 to l=0.13. To confirm the previous results on the evolution of the formation of new single-bonds, we will then calculate the Wiberg indices by NBO calculation.

Table 3. Variation of the bonding distances formed at the transition state (in Å).

Structure	C_4-N_1		C_5-N_2		Δ*l*
	r(A°)	*l*	r(A°)	*l*	
TS1	2.73	0.13	1.88	0.71	0.58
P1	1.46		1.46		
TS2	2.74	0.12	1.89	0.70	0.58
P2	1.46		1.46		
TS3	2.72	0.13	1.87	0.71	0.58
P3	1.46		1.46		
TS4	2.72	0.13	1.86	0.72	0.58
P4	1.46		1.46		
TS5	2.72	0.13	1.81	0.76	0.62
P5	1.46		1.46		
TS6	2.75	0.11	1.91	0.71	0.57
P6	1.46		1.46		

Analysis of the TV transition vectors provides valuable information on the mechanistic pathways involved in the transition states examined. Specifically, **Table** 4 presents the calculated imaginary frequencies, the most significant components of the transition vectors and their associated geometric parameters that define the structure of the transition states (TS).

Table 4. Imaginary frequency (cm^{-1}), unique Hessian eigenvalue (a. u), principal components of the transition vector (a. u) and corresponding geometric parameters (lengths in Angstrom) for the TS corresponding to the six Diels-Alder reactions.

	TS1		TS2	
	υ=356.60i; -0.0137		**υ=350.51i; -0.0198**	
N_2-C_5	0.545	1.882	**TS3**	**TS4**
C_1-C_{12}	-0.082	1.402	υ =360.36i;	υ =362.67i;
N_1-C_4	0.098	2.732	-0.0210	-0.0213
C_2-C_9	-0.022	1.366		
N-N	-0.084	1.292		
C-N-C	-0.022	126.03	**TS5**	**TS6**
N-C_{12}-H	-0.155	109.11	υ =367.55i;	υ =342.18i;
C_2-C_1-C_{12}-H	-0.224	-109.95	-0.0222	-0.01856
H-C_{12}-C_1-C_{41}	0.101	-47.748		

The evolution of the new N_1-C_4 and N_2-C_5 single bonds explains the dominance of the TV components for the different transition state (TS) structures. The change in hybridization at the nitrogen centers and at C_4 and C_5 carbons from sp^2 to sp^3 along the cycloadditions also participates in the transition vectors in the different transition state structures due to the modification of the (C-N-C) angle. The imaginary frequency values of the TSs for the six SHDA reactions are less than (500 cm^{-1}) because of the movements of the aromatic rings and their associated heavy substituents.

3.2.3. Study of GEDT in transition state structures

The Global Electron Density Transfer (GEDT) of a reaction is calculated by summing the atomic charges (q) of the atoms in each framework at the transition state structures (TS). Mathematically, it is expressed as GEDT = Σq_f. The sign of the GEDT value indicates the direction of the electron density flux: positive values signify a transfer from the considered framework to another. This concept highlights that electron density transfer in polar reactions is a global process affecting the entire molecular system, rather than being localized between specific atoms or bonds. [48]

The global electron density transfer (GEDT) was evaluated by analyzing the natural charges of the transition state (TS) structure, obtained through natural population analysis (NPA). This analysis was conducted between the nucleophilic (diene) and electrophilic (dienophile) components involved in the investigated reactions. A positive GEDT value at the transition state indicates electron migration from the diene to the dienophile.

Fig. **2** shows the results obtained. In all the reactions studied, it shows that the diene has a nucleophilic character as long as the dienophile has an electrophilic character, confirmed by the production of global electron density transfer (GEDT) from the diene to the dienophile, in agreement with the computed reactivity indices. GEDT values at the various transition states (TS) range from 0.445 e to 0.488 e, indicating the polar nature of these transition states.

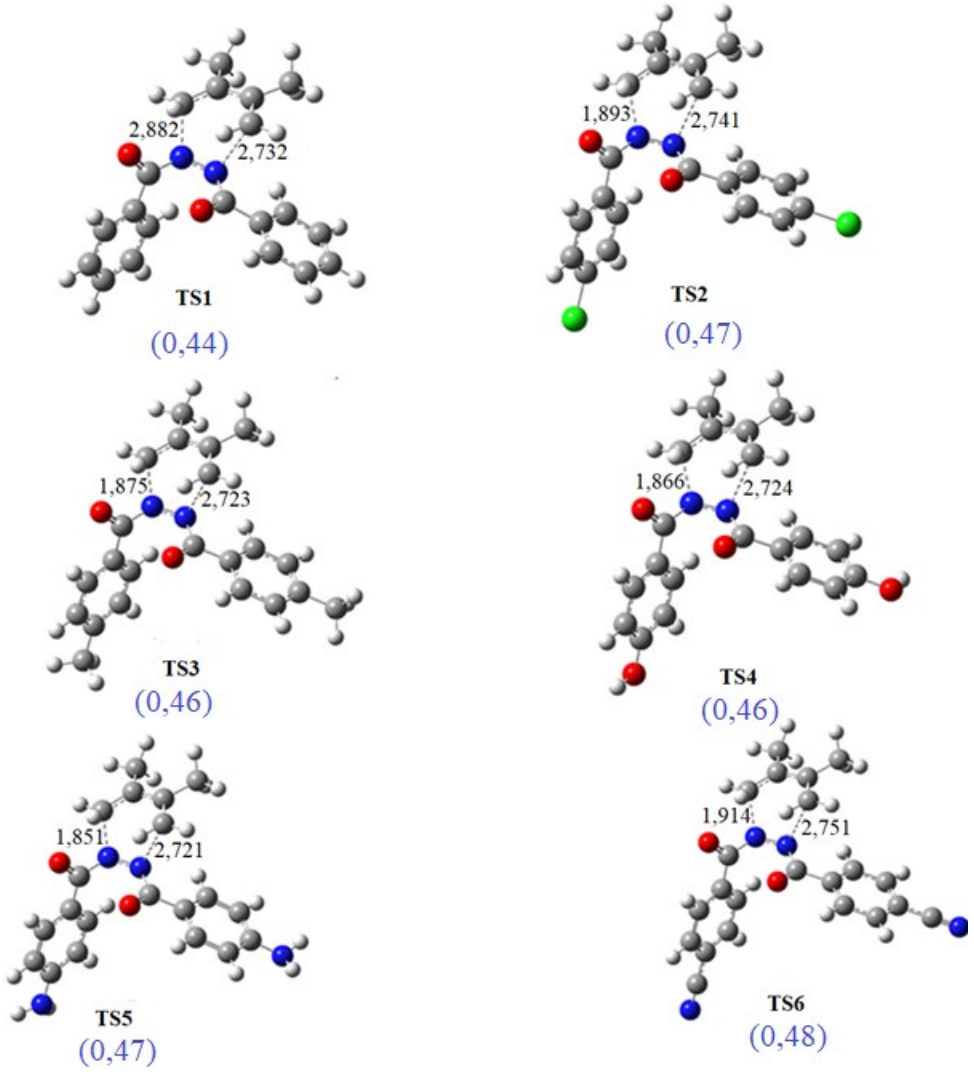

Fig. 2. Transition structures lead to the cycloadducts in the studied DA reaction. The distances of the forming bonds are given in angstroms, and Global electron density transfer (GEDT,ine).

3.3. Wiberg bond indices

The Wiberg bond indices can be used to obtain an in-depth analysis of the evolution of the cycloaddition process. These indices have been calculated using NBO natural bond orbital analysis, [49,50] and the results are presented in the additional file 1: **Table** S3. The formation percentages corresponding to new single-bonds being established at the six transition state structures (TS) transition states range from 13.35 to 15.08% for N_1-C_4 and from 51.17 to 56.01% for N_2-C_5. The evolution of N_2-C_5 bond formation is therefore premature compared with N1-C4 bond formation. In fact, the percentage difference is of the order of 42,66%, proving that the process of new bond formation is asynchronous, which is consistent with previous results concerning quantities assessing the degree of synchronicity. Yet the local descriptors of reactivity derived from CDFT are homologous for all the active sites involved in the interactions leading to the six α-aminoketone derivatives. So, a priori, the process of new bond formation must absolutely be synchronous.

3.3.1. Hydrogen Bond Length Analysis

The expected results from analysis of the CDFT parameters show that the active cities concerned by the electronic interaction are homologous on the one hand. And the complete symmetry of diene and the different dienophiles on the other hand. it is to have a synchronous process of forming new single-bonds C_5-N_2 and C_4-N_1. However, this is not the case, by the analysis of the geometries of the transition states for all the cycloaddition reactions studied via the indices of development of the bond (*l*) and the indices of Wiberg show that it is a question of an asynchronous process. To substantiate these results, geometrical analysis was performed by monitoring the remote interaction of the hydrogen atom (C-H) attached to the diene and the carbonyl (C=O) attached to the dienophile the results obtained are grouped in **Table** 5.

A breakdown of these results (**Table** 5) shows that the hydrogen bond length along the IRC pathway varies from 2.19 to 2.23 Å at the different transition state structures (TS). These bonds are shorter than those reported in the literature (2.3-3.0 Å), [42–44] which are energetically stronger. Therefore, the temporal establishment of the non-classical hydrogen bond (C=O----H–C) for all the transition state structures (TS) balances the electron density towards the carbonyl interrogated in the formation of this bond, which causes a deformation of the electronic cloud resulting in the decrease of the activation barrier (ΔE) and the increase of the dienophile electrophilicity. Recent DFT studies have shown that the formation of classical hydrogen bonds [51] (C=O----H–O) and non-classical[52,53] (C=O----H–C) to carbonyl compounds accelerates the kinetics of the DA reaction by their conversion into a more polar process due to the increase in the electrophilic power of the reactive fragment. [54,55]

Table 5. Length (in A°) of the hydrogen bond through the IRC path for the studied reactions at B3LYP / 6-311G (d, p) level.

Reaction	C –H---O=C (A°)						
	S1	S2	S3	TS	S4	S5	S6
a+b1	3.689	3.544	2.418	2.227	2.265	2.473	2.859
a+b2	2.912	2.435	2.309	2.223	2.328	2.379	2.835
a+b3	3.938	2.844	2.293	2.219	2.324	2.376	2.807
a+b4	2.384	2.239	2.205	2.212	2.286	2.395	2.775
a+b5	3.300	2.744	2.274	2.200	2.273	2.420	2.748
a+b6	3.349	2.834	2.299	2.234	2.312	2.470	2.894

3.3.2. ELF topological analysis

Several theoretical works on Diels Alder-type cycloaddition reactions have shown that the analysis of bonds by the electron localization function (ELF) [17,56,57] along the IRC reaction rate is a relevant topology to reveal the bonds that form or break during the chemical reaction. The ELF analysis confirms the presence of both bonding and non-bonding electron pairs by identifying regions, or basins, where the probability of finding localized electron density is at its maximum. The classifying these basins according to their synaptic order provides insight into the nature of electron localization. Monosynaptic pools, denoted by V(A), are generally associated with lone pairs or bond-free regions, while desynaptic pools, represented by V(A, B), correspond to binding regions shared between two atomic centers, A and B. This distinction is consistent with the Lewis bonding model and provides a clear, intuitive graphical representation of molecular electronic structure.

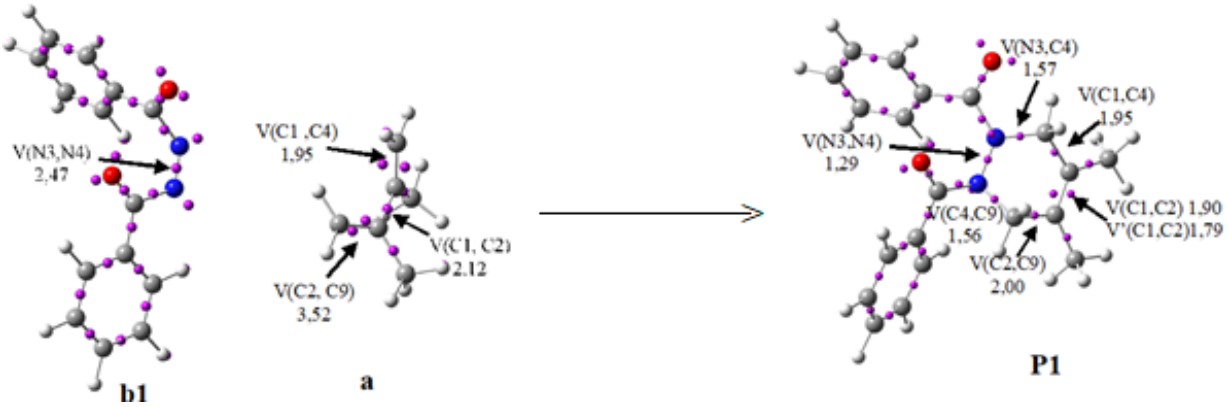

Fig. 3. ELF attractors positions of reagents (**a** and **b1**) and product (**P1**) at B3lyp/6-311G (d, p).

ELF analysis of the bonds formed and broken along the IRC path of the **a+b1** reaction, where the dienophile is not substituted (**Fig**. **3**), was carried out to highlight the electronic changes during the formation of the new N_4-C_9 and N_3-C_4 single-bonds. Indeed, the electronic populations of the most significant ELF valence basins of the selected structures are collected in the additional file 1: **Table** S4 and the attractor positions of the selected IRC path points are shown in **Fig**. 4.

The topological analysis of the ELF of the structure (S_0), shows the existence of two significant disynaptic basins V (C9, C2) and V (C4, C1) with a total population of electronic devices equal to 3,5e and tends green to 2e in the S6 structure indicating that the two bonds transform into a single-bond, in addition, we have another disynaptic basin V(N3, N4) integrating a population total of 2.47e, which decreases over the IRC path and tends towards a value of 1.29e which confirms the change to a single-bond.

The most significant monosynaptic basins are V(N3), V(N4) and V'(N4) which include 2.75 e; 2.54e; 0.69e respectively. The values of V(N3); V(N4) indicate the existence of a lone pair on atom N. The change of basin V(N3) is more remarkable at the transition state structure (TS), where the formation of the first bond (C_4-N_3) is observed. On the other hand, the two disynaptic basins V(C1, C2) and V'(C1, C2) appear at structure S7, which are worth 1,90e and 1,79e respectively, clearly showing the generation of a double bond.

From a topological point of view, the hydrogen atom is a special case, because the electron is considered as a valence electron. The monosynaptic basin C(H) does not exist and the hydrogen is therefore taken into account in the bond it forms with another atom. For example, for a C-H bond, the basin corresponding to hydrogen is denoted V(H, C), and is called protonated disynaptic basin.[57,58,59] Thus, the basins number C(O8), C(N3), and C(C12) indicate the presence of a temporal hydrogen bond which is formed in particular at the structure S4 such that the basin V(C12, H14)integrates a value of 1,98e and the disynaptic basin V(C2,N5) at a value of 2.85e, which clearly explains the interaction induced by this bond, meaning that hydrogen is inserted in the in the non-classical hydrogen bond formation (C=O----H-C).

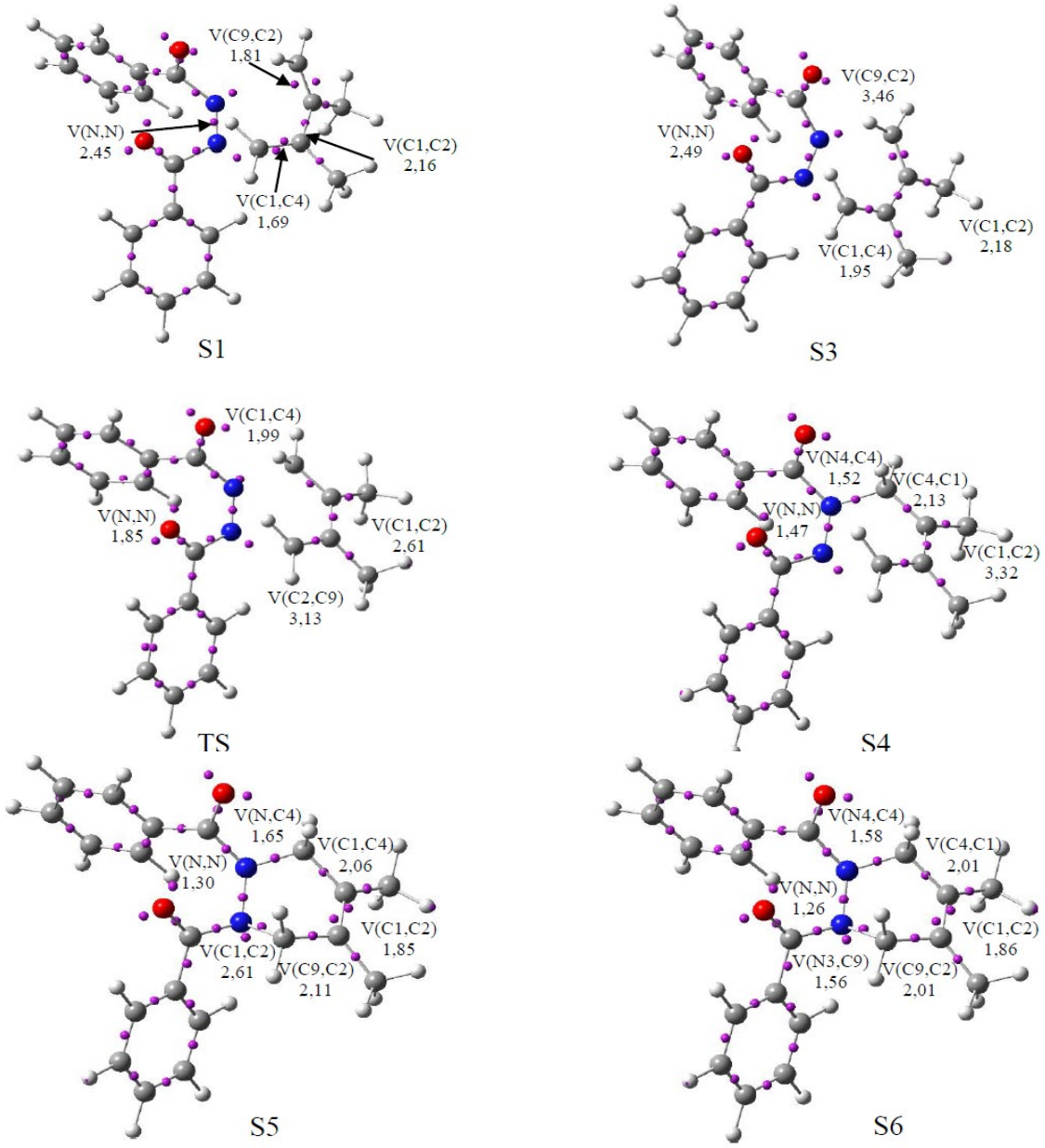

Fig. 4. ELF attractors positions of different points selected from the IRC path of the favorable product (P1) at B3LYP/6-311G (d, p).

3.4. Exploration of the interactions between derivatives compounds of the pyridazine family and the main protease Mpro of HIV-1

Human immunodeficiency virus type 1 (HIV-1) is associated with a transient symptomatic illness marked by high levels of viral replication and a vigorous immunological response to the infection. Between 40% and 90% of new HIV-1 infections present with symptoms. However, this condition is often undiagnosed or misdiagnosed because anti-HIV-1 antibodies are usually undetectable during the early stages of infection. Accurate diagnosis of acute HIV-1 infection requires strong clinical suspicion and appropriate laboratory diagnostic tests. [60] According to the World Health Organization (WHO), approximately 38 million individuals were living with HIV globally in 2021. Among them, 1.7 million were children under the age of 15, and about 54% of the affected population consisted of women and girls. Currently, there are several antiviral agents available to treat this disease when it is diagnosed early. [61,62] In this context, certain organic compounds, particularly those from the pyridazine family, may hold promise for treating this disease. Pyridazine derivatives are notable among nitrogen-containing heterocycles due to their wide range of pharmacological activities. These include antibacterial, muscle relaxant, antidepressant, antidiabetic, antihypertensive, analgesic, antitumor, antiviral, nephroprotective, anti-inflammatory, anti-aggregant, antiepileptic, and anticancer properties. [63,64]

Table 6. Binding energy and interactions of the top scoring products (P1-P6) with HIV-1 protein.

Target-Protein	Compounds	Amine acids	Position	Distance	Interaction type	Binding Energy score (kcal/mol)
4DJO	P1	VAL	82	5.12	Alkyl	-10.5
		PRO	81	4.77		
		PHE	53	5.12		
		ARG	8	3.66	Pi-Cation	
		ASP	29	3.79	Pi-Anion	
		MK	5101	3.43	Pi-Sigma	
		PHE	53	5.10	Pi-Pi-shaped	
	P2	PRO	81	4.95-4.63	Alkyl	-10.7
		VAL	82	5.45		
		PHE	53	4.89-5.21		
		LEU	23	3.80		
		ARG	8	3.61	Pi-Cation	
		ASP	29	3.78	Pi-Anion	
		MK	5101	3.52	Pi-sigma	
		PHE	53	4.92	Pi-Pi T-shaped	
	P3	PRO	81	4.78-5.05	Alkyl	-10.9
		VAL	82	5.37		
		PHE	53	4.80-5.26		
		LEU	23	3.59		
		ARG	8	3.61	Pi-Cation	
		ASP	29	3.72	Pi-Anion	
		MK	5101	3.52	Pi-sigma	
		PHE	53	4.93	Pi-Pi T-shaped	
	P4	PRO	81	4.88-4.89	Alkyl	-10.4
		VAL	82	5.30		
		PHE	53	5.09		
		ARG	8	3.64	Pi-Cation	
		ASP	29	3.71	Pi-Anion	
		MK	5101	3.51	Pi-sigma	
		PHE	53	4.92	Pi-Pi T-shaped	
	P5	PRO	81	4.73-4.96	Alkyl	-10.3
		VAL	82	5.30		
		PHE	53	4.93		
		ARG	8	3.65	Pi-Cation	
		MK	5101	3.53	Pi-sigma	
		PHE	53	4.99	Pi-Pi T-shaped	
		ASP	29	2.72	Conventional Hydrogen Bond	
		GLY	27	2.74		
	P6	PRO	81	4.98-5.01	Alkyl	-10.2
		VAL	82	5.31		
		PHE	53	5.33		
		ARG	8	3.65	Pi-Cation	
		MK	5101	3.71	Pi-sigma	
		PHE	53	4.73	Pi-Pi T-shaped	
		GLY	48	2.83	Conventional Hydrogen Bond	
Drug Standard	Amprenavir					-7.85

Despite the potential of the six pyridazine derivatives (**Fig**. S2), they had not been experimentally tested against HIV-1 prior to this study. Therefore, we performed, for the first time, modeling using AutoDock to estimate the effectiveness of these derivatives against HIV-1's main protease (Mpro), in complex with MKP56 (**Fig**. S3). The 4DJO series represents a new class of HIV-1 protease inhibitors designed using a strategy that combines structure-based design with substrate-envelope constraints. These inhibitors incorporate various P2 carbamates derived from alcohols, featuring both acyclic and cyclic heteroatomic functionalities within the (R)-hydroxyethylamine isostere. Molecular docking studies are valuable usefull tool[65] that provides insights into the potential electronic affinity achieved by ligands or products interacting with a protein (Mpro).The crystal structure of wild-type HIV-1 protease in complex with MKP56 [66] has been examined. The biological

activity against HIV-1 (AIDS) of the six pyridazine compounds was assessed using AutoDock tools with the Lamarkian genetic algorithm [67] Herein, Amprenavir(CID: 65016) was employed as a standard for docking studies against. target proteins due to its inhibitory activity against HIV-1 previously reported. [68] **Fig. 5** and **6** show the three-dimensional and two-dimensional structures, respectively, depicting the interactions between the products and the protein binding site. **Table 6** provides details on the interactions between the key residues (amino acids) of the protein and the six products. From **Fig. 6**, it is clear that the carbon atoms of compounds P1-P4 form alkyl bonds with PRO-81 (at distances of 4.63 Å and 4.95 Å), VAL-82 (5.30 Å and 5.45 Å), and PHE-53 (4.80 Å and 5.26 Å). Additionally, these compounds establish Pi-Cation bonds with ARG-8 at distances of 3.66 Å (P1), 3.61 Å (P2), 3.61 Å (P3), and 3.64 Å (P4). Likewise, for compounds P1-P4, three types of interactions are noted: a Pi-anion bond with ASP-29 at distances of 3.79 Å (P1), 3.78 Å (P2), 3.72 Å (P3), and 3.71 Å (P4); a Pi-sigma interaction with MK-5101 at distances of 3.43 Å (P1), 3.52 Å (P2), 3.52 Å (P3), and 3.52 Å (P4); and a Pi-Pi T-shaped bond with PHE-53 at distances of 5.10 Å (P1), 4.92 Å (P2), 4.93 Å (P3), and 4.92 Å (P4). For products P5 and P6, interactions occur with PRO-81 at distances between 4.73 and 4.96 Å for P5 and between 4.98 and 5.01 Å for P6. Interactions with VAL-82 are observed at 5.30 Å for P5 and 5.31 Å for P6. Alkyl bonds with PHE-53 are noted at 4.93 Å for P5 and 5.33 Å for P6. Additionally, Pi-Cation and Pi-sigma interactions are seen with ARG-8 and MK-5101, respectively, at distances of 3.65 Å for both interactions in P5, and 3.65 Å and 3.71 Å for P6. Moreover, a Pi-Pi T-shaped bond with PHE-53 is noted at approximately 4.99 Å for P5 and 4.73 Å for P6. Additionally, conventional hydrogen bonds form with amino acid residues ASP-29 and GLY-27, at distances of 2.72 Å and 2.74 Å for P5, and with GLY-48 at 2.83 Å. Molecular docking studies with 4DJO reveal that all products (P1-P6) exhibit high binding energy values of −10.5, −10.7, −10.9, −10.4, −10.3, and −10.2 kcal/mol, respectively. These results suggest a strong binding affinity of the compounds to 4DJO, which may hinder substrate accessibility and potentially lead to inhibition.

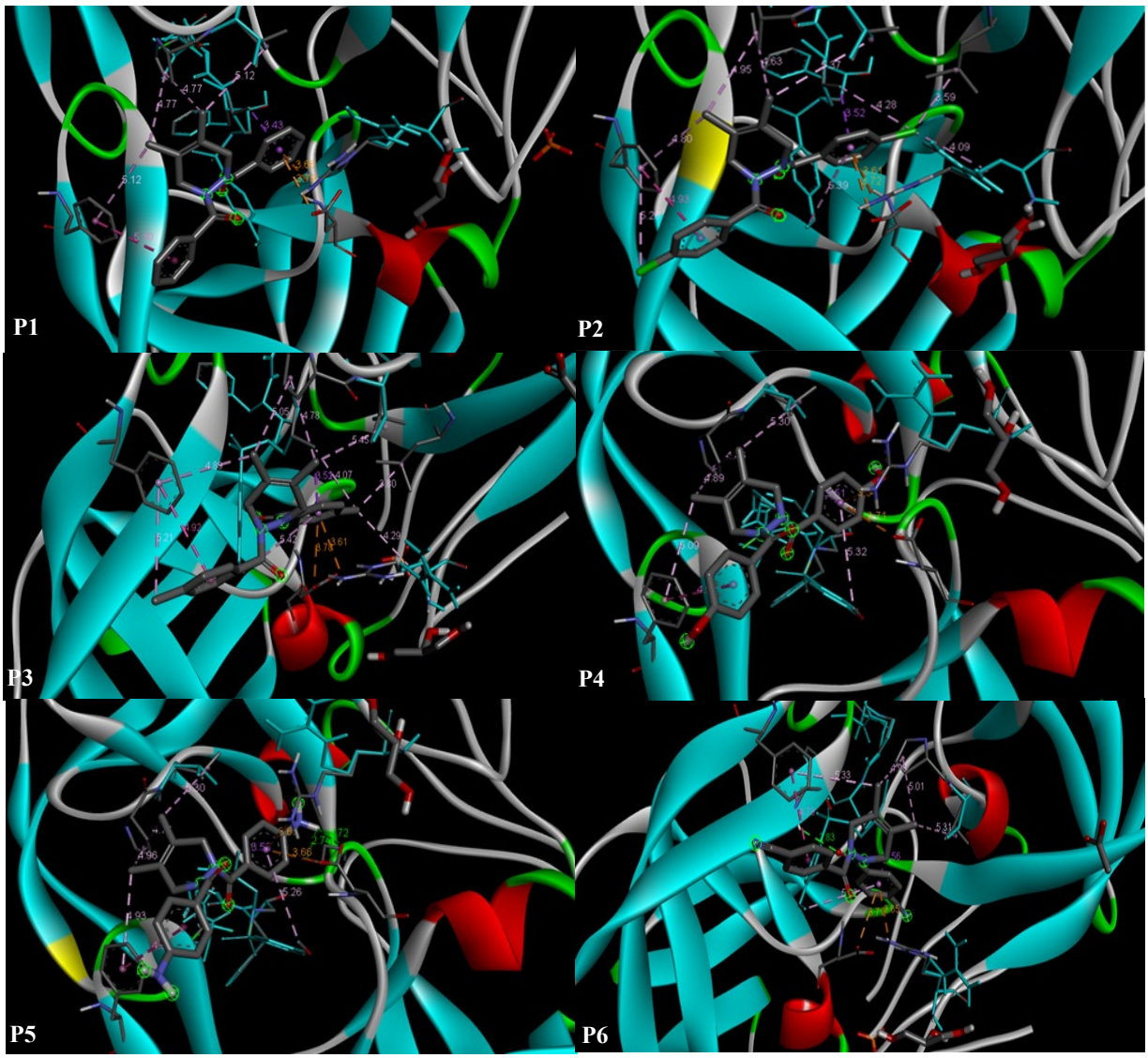

Fig. 5. 3D structures of interaction of the six products with the target protein (4DJO) of HIV-1.

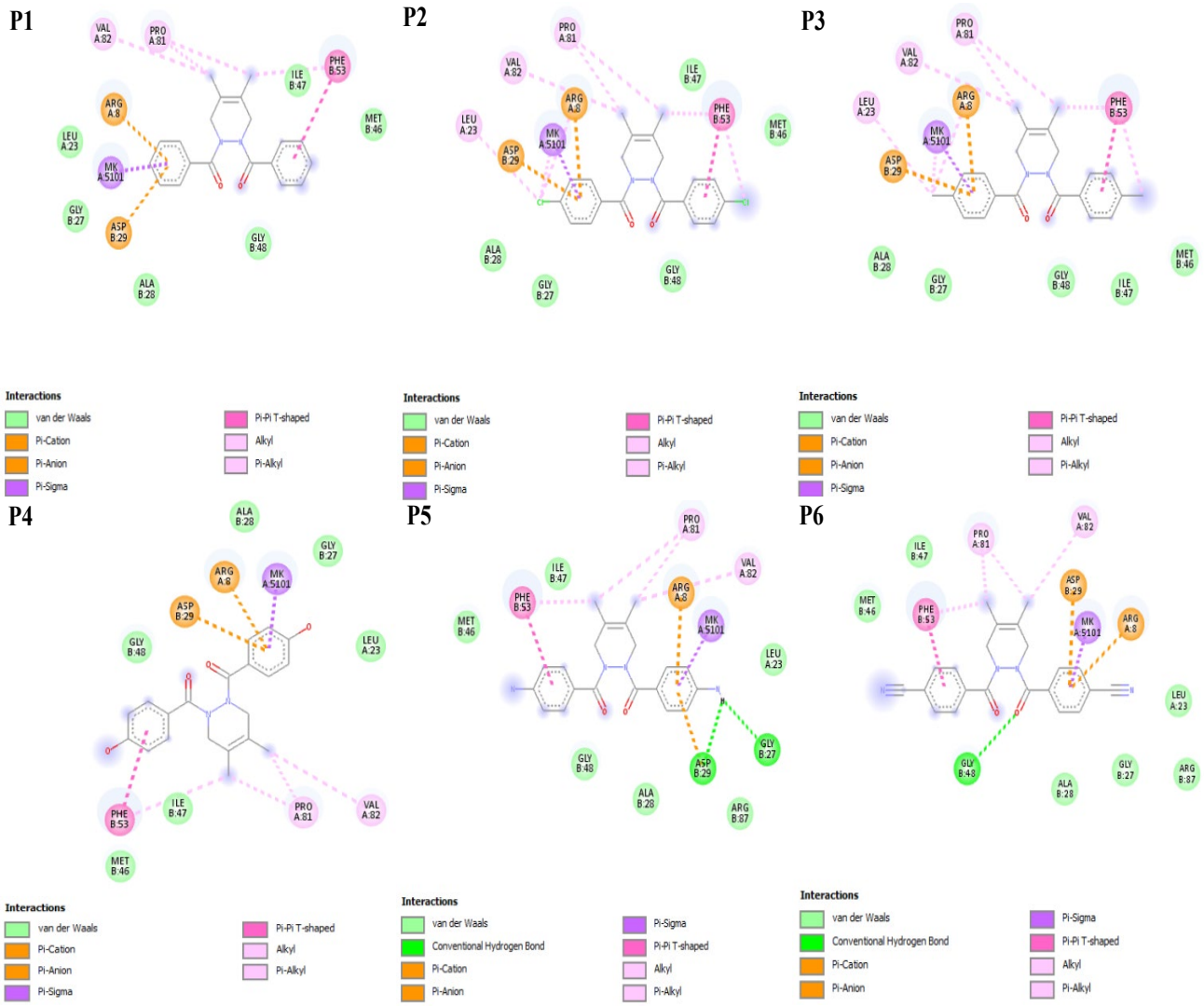

Fig. 6. 2D structures of interaction of the six products with the target protein (4DJO) of HIV-1.

3.5. Prediction of ADMET and related properties

Every year, a multitude of bioactive molecules are unearthed, but their clinical application and optimal use are invariably dictated by pharmacokinetic and toxicity parameters. The effectiveness of a drug hinges on its ability to reach its specific target within the body at a sufficient concentration and maintain its bioactive state long enough to produce the desired biological effects. Therefore, the practical viability of a potential drug candidate primarily depends on its absorption, distribution, metabolism, excretion, and toxicity (ADMET) profile. [69] The acceleration of drug discovery can be markedly enhanced by initially prioritizing computational studies to evaluate the ADMET profiles and docking efficiency of key compounds.

3.5.1. Gastrointestinal absorption (GIA) prediction

The ability of the small intestine to absorb orally administered drugs plays a crucial role in determining a drug's bioavailability. After administration, the amount of drug reaching the portal vein is commonly used as an indicator of intestinal absorption. This method reduces the impact of metabolic transformations, as drugs often undergo hepatic transformation before entering the systemic circulation. In the present study, the GIA descriptor was calculated using the pkCSM tool, enabling prediction of drug absorption rates across the human intestinal barrier. A thorough review of the existing literature highlights that more likely to penetrate the intestinal barrier are molecules or drugs with absorption rates exceeding 30% . [70] Taking this into account, the results displayed **Table** S5 provide significant insights. All P1-P6 compounds demonstrate substantial absorption rates, ranging from 85.27% to 97.42%. This suggests that compounds in this category show promising potential as candidates for oral drug development.

3.5.2. Prediction of BBB permeability "Distribution"

The blood-brain barrier acts as a protective shield for the central nervous system (CNS) by regulating the entry of blood into cerebral tissues. Comprising the cerebral endothelium, this barrier selectively controls the passage of molecules of different sizes into the CNS. It allows entry only to specific transport molecules that are soluble in both water and lipids. Additionally, the barrier expresses a diverse array of active transporters, including glucose and P-gp transporters. Glucose transport into brain cells is facilitated through these glucose transporters. [71] According to the distribution results, all the compounds studied, with the exception of P1 and P3, have a blood-brain barrier permeability index (logBB) of less than 0.3. This suggests a limited capacity to cross this protective barrier, reducing the likelihood of reaching the central nervous system. At the same time, the negative values of the logPS parameter confirm the low capacity of these molecules to penetrate the brain and cross the blood–brain barrier. Consequently, their use as therapeutic agents presents little risk of neurotoxic effects or undesirable interactions with the central nervous system. This reinforces their safety profile and supports their potential as candidates for pharmaceutical development.

3.5.3. Metabolism

The ADMET bindings of CYP2D6 and CYP3A4 predict the inhibition of cytochrome P450 enzymes 2D6/3A4. Predictions are made using a probabilistic approach, based on a training dataset containing 100 compounds with established inhibition and substrate profiles towards the CYP2D6 and CYP3A4 enzymes. This method exploits the 2D chemical representation of the molecules as input data, enabling precise estimation of the metabolic behavior of the compounds studied. These descriptors determine the effect of the inhibitor and substrate by predicted classes: non-inhibitor and non-substrate (false) and inhibitor/non-substrate (true). All the compounds analyzed do not block the CYP2D6 enzyme, which means they can be well metabolized by the liver in the first phase of metabolism. This suggests that they are unlikely to cause liver-related side effects, and therefore do not present a risk of hepatotoxicity.

3.5.4. Excretion and Toxicity predictions

One of the key factors contributing to failure in the advanced stages of drug development is toxicity, which refers to the potential harm a molecule may cause to organs, cells, and tissues in the body. Early detection of toxicity would, therefore, be immensely beneficial. In this study, we assessed descriptors related to toxicity using pkCSM pharmacokinetics. The compounds (P1–P6) were not identified as substrates of the renal Organic Cation Transporter 2 (OCT2). They were subsequently evaluated using the Ames test, which indicated that all compounds were non-toxic, except for P5 and P6, which showed potential toxicity. Simultaneously, in the context of hERG I/II inhibition (hERG refers to a human gene that encodes for an ion channel involved in the transport of potassium across the cell membrane. These channels play a crucial role in regulating the action potential of the heart), with the exception of product P5, all compounds demonstrated non-toxic attributes, thereby confirming their effectiveness.

3.5.5. Drug-likeness assessment

The prediction of physicochemical parameters including topological polar surface area (TPSA), molecular weight, Log Kp (skin permeation), number of rotational bonds, donors/acceptors of hydrogen bonds, molar refractivity, lipophilicity and aqueous solubility is efficiently achieved using the Swiss-ADME server. These molecular descriptors are essential, as they directly influence a compound's pharmaceutical effectiveness. Lipophilicity, a measure of a molecule's ability to dissolve in fats, non-polar solvents, and oils, is particularly critical for its biological permeability. Optimal lipophilicity enables a drug to effectively penetrate lipid bilayers, facilitating its therapeutic action. However, excessive lipophilicity can hinder excretion, potentially leading to increased toxicity by prolonging the molecule's presence in the body. Thus, striking a balance in lipophilicity is essential for enhancing drug efficacy while minimizing the risk of adverse effects on physiological systems. [72] The partition coefficient between octanol and water (Log Po/w) serves as the chemical descriptor for lipophilicity, and Swiss-ADME provides detailed information on this aspect, utilizing five predictive models (iLOGP, XLOGP3, WLOGP, MLOGP, SILICOS-IT). XLogP3 is particularly utilized to establish the bioavailability radar. It is noteworthy that all examined analogs of isoniazide exhibit optimal lipophilicity, thus enhancing their interaction with biomembranes. The compounds studied from the pyridazine family (P1-P6), show consensus Log P/ω values estimated at 2.75, 4.07, 3.68, 2.22, 1.93, and 2.59, respectively. These values indicate that all compounds fall within the optimal range of Log P/ω ≤ 5, thereby classifying them as lipophilic drugs, [73] Based on Lipinski's rules (**Table** S6), all these compounds have molecular masses below 500 g/mol (320.39, 389.28, 348.44, 352.38, 350.41, 370.40). The number of hydrogen bond donors (HBD) for each compound is 0, 0, 0, 2, 2, 0 for P1, P2, P3, P4, P5, P6, respectively, which is less than 5. Additionally, the number of hydrogen bond acceptors (HBA) for each molecule is also below 10 (2, 2, 2, 4, 2, 4 for P1, P2, P3, P4, P5, P6, respectively), indicating satisfactory binding strength. The ability of an orally administered drug to cross biological membranes is generally assessed using topological polar surface area (TPSA). This parameter is calculated on the basis of the surface contributions of polar atoms, such as oxygen and nitrogen, as well as the hydrogen atoms attached to them. A TPSA value of less than 140 Å² is generally considered favourable to good oral bioavailability. For compounds (P1-P6), the calculated TPSA values were 40.62, 40.62, 40.62, 81.08, 92.66, and 88.20, respectively. These values indicate high permeability through the plasma membrane.[74] Another critical parameter in evaluating drug-likeness is the number of rotatable bonds (RTBs). This descriptor significantly influences both bioavailability and binding affinity, as molecules need

to adopt specific conformations to effectively bind and traverse membranes. A molecule with fewer RTBs experiences less entropy loss, which is advantageous for maintaining its stability and functionality. Therefore, for potential drug candidates, the number of RTBs should be ≤ 10. In the case of compounds P1-P6, their limited flexibility, characterized by fewer than 10 rotatable bonds (P1 (RB=0), P2 (RB=4), P3 (RB=4), P4 (RB=4), P5 (RB=4), P6 (RB=4)), suggests promising oral bioavailability. The main objective of drug development research is to determine the stage at which a molecule becomes capable of producing substances bioavailable for oral consumption. the bioavailability score (BS) is used to estimate the probability that a molecule will be well absorbed. Significantly, all the compounds examined in our study achieved a BS of around 0.55, which corresponds to the optimal range for a neutral molecule to function effectively as an oral drug[74].

4. Conclusion

Symmetric Hetero-Diels–Alder (SHDA) cycloadditions between 2,3-dimethylbutadiene and six azodicarbonyl derivatives bearing electron-donating or electron-withdrawing groups were theoretically investigated using the B3LYP/6-311G(d,p) method. Energy and geometric parameters were calculated in both gas and condensed phases. Local reactivity indices revealed minimal impact of para-substitution on electrophilicity and nucleophilicity. The chemical potential values indicated an electronic flow from the diene to the dienophile. Wiberg bond indices showed asynchronous bond formation, and ELF analysis confirmed a concerted, single-step mechanism. These reactions were classified as polar or moderately polar based on GEDT, activation barriers, and electrophilicity variation. Asynchronicity was attributed to steric and π-delocalization effects, supported by the presence of a transient non-classical hydrogen bond at the transition state. This interaction delays one bond formation until the weakening of another. Molecular docking identified six potential HIV-1 inhibitors, with five showing favorable ADMET profiles. The compound (4,5-dimethyl-3,6-dihydropyridazine-1,2-diyl) bis(p-tolylmethanone) was most promising, warranting further in vitro, in vivo, and clinical studies.

Competing of interests: The authors declare that they do not have any competing interests.

Declarations Funding: The authors received no specific funding for this work.

1. **Conflicts of interest/Competing interests:** The authors declare that they have no conflict of interest and no competing interests exist.
2. **Ethics approval:** The manuscript is prepared in compliance with the Ethics in Publishing Policy as described in the Guide for Authors.
3. **Consent for publication:** The consent for publication was obtained from all participants.
4. **Availability of data and material:** All data generated or analyzed during this study are included in this published article.

Authors' contributions: Mohamed Sahrane, Tarik Boutadghart, A. Arif and R. Ghilane: Article Writing. M. El idrissi and R. Ghilane: numerical calculations. M. El idrissi and I. Mennas: Final review and editing.

References

1. Jasiński R. **(2024)** Synthesis of 1,2-oxazine N-oxides via noncatalyzed hetero-Diels–Alder reactions of nitroalkenes (microreview). *Chem. Heterocycl. Compd*. 60(3), 121–123. https://doi.org/10.1007/s10593-024-03047-4
2. Matiichuk Y., Drapak I., Darmograi N., Bartoshyk N., Drapak Y., & Matiychuk V. **(2024)** Nitro-functionalized analogues of 1,3-Butadiene: An overview of characteristics, synthesis, chemical transformations and biological activity. *Curr. Chem. Lett.* 13, 15–30. https://doi.org/10.5267/j.ccl.2023.9.003
3. Nicolaou K.C., Snyder S.A., Montagnon T., & Vassilikogiannakis G. **(2002)** The Diels–Alder reaction in total synthesis. *Angew. Chem. Int. Ed.* 41(10), 1668–1698. https://doi.org/10.1002/1521-3773(20020517)41:10<1668::AID-ANIE1668>3.0.CO;2-Z
4. Parr R.G., Szentpály L.V., & Liu S. **(1999)** Electrophilicity index. *J. Am. Chem. Soc*. 121(8), 1922–1924. https://doi.org/10.1021/ja983494x
5. Parr R.G., & Yang W. **(1989)** Density Functional Theory of Atoms and Molecules. (Book chapter) *Oxford University Press*. https://doi.org/10.1007/978-94-009-9027-2_2
6. Domingo L.R., Ríos-Gutiérrez M., & Pérez P. **(2025)** Electrophilicity ω and Nucleophilicity N scales for cationic and anionic species. *Scientiae Radices* 4(1), 1–17. https://doi.org/10.58332/scirad2025v4i1a01 sci-rad.com+2sci-rad.com+2
7. Domingo L. **(2016)** Molecular electron density theory: A modern view of reactivity in organic chemistry. *Molecules* 21(10), 1319. https://doi.org/10.3390/molecules21101319
8. Pérez P., Domingo L.R., Aizman A., & Contreras R. **(2007)** The electrophilicity index in organic chemistry. *Theor. Comput. Chem*. 19, 139–201. https://doi.org/10.1016/S1380-7323(07)19009-2
9. Pérez P., Domingo L.R., Duque-Noreña M., & Chamorro E. **(2009)** A condensed-to-atom nucleophilicity index. *J. Mol. Struct.*: *THEOCHEM* 895(1–3), 86–91. https://doi.org/10.1016/j.theochem.2008.10.014

10. Domingo L.R., Pérez P., & Sáez J.A. **(2013)** Understanding the local reactivity in polar organic reactions through electrophilic and nucleophilic Parr functions. *RSC Adv*. 3(4), 1486–1494. https://doi.org/10.1039/C2RA22886F
11. Domingo L.R., & Sáez J.A. **(2009)** Understanding the mechanism of polar Diels–Alder reactions. *Org. & Biomol. Chem.* 7, 3576–3585 (estimation). https://doi.org/10.1039/b909611f
12. Diez-Martinez A., Tejero T., & Merino P. **(2010)** Experimental and theoretical studies on Mannich-type reactions of chiral non-racemic N-(benzyloxyethyl) nitrones. *Tetrahedron: Asymmetry* 21(22), 2934–2943. https://doi.org/10.1016/j.tetasy.2010.12.004
13. Zeroual A., Ríos-Gutiérrez M., El idrissi M., El Alaoui El Abdallaoui H., & Domingo L.R. **(2019)** An MEDT study of the mechanism and selectivities of the [3+2] cycloaddition reaction of tomentosin with benzonitrile oxide. *Int. J. Quantum Chem.* 119(18), e25980. https://doi.org/10.1002/qua.25980
14. Jasiński R**. (2015)** A stepwise, zwitterionic mechanism for the 1,3-dipolar cycloaddition between (*Z*)-*C*-4-methoxyphenyl-*N*-phenylnitrone and *gem*-chloronitroethene catalysed by 1-butyl-3-methylimidazolium ionic liquid cations. *Tetrahedron Lett*. 56(3), 532–535. https://doi.org/10.1016/j.tetlet.2014.12.007
15. Jasiński R., Kubik M., Łapczuk-Krygier A., Kącka A., Dresler E., & Boguszewska-Czubara A. **(2014)** An experimental and theoretical study of the hetero Diels–Alder reactions between (E)-2-aryl-1-cyano-1-nitroethenes and ethyl vinyl ether: one-step or zwitterionic, two-step mechanism*? Reaction Kinet. Mech. Catal.* 113, 333–345. https://doi.org/10.1007/s11144-014-0753-8
16. Atif M., Barhoumi A., Syed A., Bahkali A.H., Chafi M., Zeroual A., Ahamad Paray B., Wang Sh., & El idrissi M. **(2024)** ADME study, molecular docking, elucidating the selectivities and the mechanism of [4+2] cycloaddition reaction between (E)-N((dimethylamino)methylene)benzothioamide and (S)-3-acryloyl-4-phenyloxazolidin-2-one. *Mol. Biotechnol*. **67**, 1065–1076. https://doi.org/10.1007/s12033-024-01105-w
17. Barhoumi A., Elkacmi R., Ouled Aitouna A., Zeroual A., & El idrissi M. **(2020)** Mechanistic study of hetero-Diels–Alder [4+2] cycloaddition reactions between 2-nitro-1H-pyrrole and isoprene*. Chem. Afr*. 3, 901–909. https://doi.org/10.1007/s42250-020-00187-8
18. Jasiński R. **(2014)** Searching for zwitterionic intermediates in hetero Diels–Alder reactions between methyl α,β-dinitrocinnamate and vinyl-alkyl ethers. Comput. *Theor. Chem.* 1046, 93–98. https://doi.org/10.1016/j.comptc.2014.08.002
19. Boutadghart T., & Ghailane R. **(2023)** A molecular electron density theory study of asymmetric Diels–Alder [4+2] reaction's mechanism of furan with three substituted alkynes (5-R substituted-3-(3-(phenylsulfonyl)-propioloyl)-oxazolidin-2-one). *J. Mol. Model*. 29, 290. https://doi.org/10.1007/s00894-023-05665-7
20. Boger D.L., & Weinreb S.M. **(2012)** Hetero Diels-Alder methodology in organic synthesis. *Elsevier Science: Saint Louis.* ISBN 978-0-08-091697-2
21. Boger D.L. **(1987)** Hetero Diels-Alder methodology in organic synthesis. *Org. Chem. Ser. Monogr.* 47, 300–310. https://doi.org/10008932336
22. Sakurai M., Kihara N., Watanabe N., Ikari Y., & Takata T. **(2018)** Synthesis of α-aminocarbonyl compounds via hetero Diels–Alder reaction. *Chem. Lett.* 47(1), 144–147.
23. Sakurai M., & Kihara N. **(2019)** Thermally stable Diels–Alder polymer using an azodicarbonyl compound. *Polymer* 167, 60–66.
24. Haaland A., Shorokhov D.J., & Tverdova N.V. **(2004)** Topological analysis of electron densities: Is the presence of an atomic interaction line in an equilibrium geometry a sufficient condition for the existence of a chemical bond? *Chem. – Eur. J.* 10, 4416–4421. https://doi.org/10.1002/chem.200400663
25. Domingo L.R., Chamorro E., & Pérez P. **(2010)** Understanding the mechanism of non-polar Diels–Alder reactions. *Org. & Biomol. Chem*. 8(24), 5495–5504. https://doi.org/10.1039/c0ob00563k
26. Barone V., Cossi M., & Tomasi J. **(1998)** Geometry optimization of molecular structures in solution by PCM. *J. Comput. Chem*. 19(4), 404–417. https://doi.org/10.1002/(SICI)1096-987X(199803)19:4<404::AID-JCC3>3.0.CO;2-W
27. Koubi Y., Moukhliss Y., Hajji H., Abdessadak O., Alaqarbeh M., Ajana M, Maghat H., Lakhlifi T., & Bouachrine M. **(2024)** Computational structure–biological activity and retrosynthesis investigations of 1,2,3-triazole–quinoline hybrid molecules as potential respiratory virus inhibitors. *Chem. Heterocycl. Compd*. 60, 491–504. https://doi.org/10.1007/s10593-024-03367-3
28. Wei J., Chen L., Zhu K., Cheng Y.X., & Huang D. **(2024)** Design, synthesis, and fungicidal activity evaluation of 2-methyl-5-phenylthiazole-4-carboxamides bearing morpholine, thiomorpholine, or thiomorpholine 1,1-dioxide moiety. *Chem. Heterocycl. Compd*. 60, 536–543. https://doi.org/10.1007/s10593-024-03372-6
29. Molchanova M.V., Ikonnikova V.A., Anisenko A.N., Gottikh M.B., Baranov M.S., & Mikhaylov A.A **(2024)** The cycloaddition reaction of benzothiazolium ylides with α-cyanocinnamamides: the synthesis of structural analogs of inhibitors of HIV-1 post-integrational repair**.** *Chem. Heterocycl. Compd.* 60, 544–548. https://doi.org/10.1007/s10593-024-03373-5
30. Cossi M., Barone V., Cammi R., & Tomasi J. **(1996)** Ab initio study of solvated molecules: A new implementation of PCM. *Chem. Phys. Lett.* 255, 327–335. https://doi.org/10.1016/0009-2614(96)00349-1
31. Savin A., Silvi B., & Colonna F. **(1996)** Topological analysis of the electron localization function applied to delocalized bonds*. Can. J. Chem.* 74, 1088–1096. https://doi.org/10.1139/v96-122
32. Lu T., & Chen F. **(2012)** Multiwfn: A multifunctional wavefunction analyzer. *J. Comput. Chem*. 33(5), 580–592. https://doi.org/10.1002/jcc.22885

33. Wang H., He H., Zhang T., & Jiang J. **(2022)** Application of Reverse Docking in the Research of Small Molecule Drugs and Traditional Chinese Medicine. *Biol. Pharm. Bull.* 45(1), 19–26.10.1248/bpb.b21-00324
34. Nguyen N.T., Nguyen T.H., Pham T.N.H., Huy N.T., Bay M.V., Pham M.Q., Nam P.C., Vu V.V., & Ngo S.T. **(2020)** Autodock Vina adopts more accurate binding poses but Autodock4 forms better binding affinity. *J. Chem. Inf. Model*. 60(1), 204–211. https://doi.org/10.1021/acs.jcim.9b00778
35. Lee A., Lee K., & Kim D. **(2016)** Using reverse docking for target identification and its applications for drug discovery. *Expert Opin. Drug Discov.* 11(8), 707–715. https://doi.org/10.1080/17460441.2016.1190706
36. Reed A.E., Weinstock R.B., & Weinhold F. **(1985)** Natural population analysis. *J. Chem. Phys.* 83(2), 735–746. https://doi.org/10.1063/1.449486
37. Jasiński R. **(2016)** First example of stepwise, zwitterionic mechanism for bicyclo[2.2.1]hept-5-ene (norbornene) formation process catalyzed by the 1-butyl-3-methylimidazolium cations. *Monatsh. Chem*. 147(7), 1207–1213. https://doi.org/10.1007/s00706-016-1735-5
38. Jasiński R. **(2015)** Nitroacetylene as dipolarophile in [2+3] cycloaddition reactions with allenyl-type three-atom components: DFT computational study. *Monatsh. Chem.* 146(4), 591–599. https://doi.org/10.1007/s00706-014-1389-0
39. Chang M.W., Ayeni C., Breuer S., & Torbett B.E. **(2010)** Virtual screening for HIV protease inhibitors: a comparison of AutoDock 4 and Vina. *PLoS ONE* 5(8), e11955. DOI: 10.1371/journal.pone.0011955
40. Schiffrin B., Radford S.E., Brockwell D.J., & Calabrese A.N. **(2020)** PYXLINKVIEWER: a flexible tool for visualization of protein chemical crosslinking data within the PyMOL molecular graphics system. *Protein Sci*. 29(6), 1851–1857. https://doi.org/10.1002/pro.3902
41. BIOVIA D.S. **(2016)** Discovery Studio. *Dassault Systèmes BIOVIA*.
42. Wu P., Lin S., Cao G., Wu J., Jin H., Wang C., Wong M.H., Yang Z., & Cai Z. **(2022)** Absorption, distribution, metabolism, excretion and toxicity of microplastics in the human body and health implications. *J. Hazard. Mater.* 437, 129361. https://doi.org/10.1016/j.jhazmat.2022.129361
43. Pires D.E.V., Blundell T.L., & Ascher D.B. **(2015)** pkCSM: predicting small-molecule pharmacokinetic and toxicity properties using graph-based signatures. J. Med. Chem. 58(9), 4066–4072. https://doi.org/10.1021/acs.jmedchem.5b00104
44. Yadav A.R., & Mohite S.K. **(2020)** ADME analysis of phytochemical constituents of Psidium guajava. *Asian J. Res. Chem.* 13(5), 373–375. https://doi.org/10.5958/0974-4150.2020.00070.X
45. Domingo L., Ríos-Gutiérrez M., & Pérez P. **(2016)** Applications of the conceptual density functional theory indices to organic chemistry reactivity. *Molecules* 21(6), 748. https://doi.org/10.3390/molecules21060748
46. Domingo L.R., Aurell M.J., Pérez P., & Contreras R. **(2002)** Quantitative characterization of the global electrophilicity power of common diene/dienophile pairs in Diels-Alder reactions. *Tetrahedron* 58(22), 4417–4423. https://doi.org/10.1016/S0040-4020(02)00410-6
47. Domingo L.R., Ríos-Gutiérrez M., & Pérez P. (2017) How does the global electron density transfer diminish activation energies in polar cycloaddition reactions? A MEDT study. *Tetrahedron* 73, 1718–1724. https://doi.org/10.1016/j.tet.2017.02.012
48. Sudha S., Sundaraganesan N., Vanchinathan K., Muthu K., & Meenakshisundaram S.P. **(2012)** Spectroscopic (FTIR, FT-Raman, NMR and UV) and molecular structure investigations of 1,5-diphenylpenta-1,4-dien-3-one: A combined experimental and theoretical study. *J. Mol. Struct*. 1030, 191–203. https://doi.org/10.1016/j.molstruc.2012.04.030
49. Harris T.K., & Mildvan A.S. **(1999)** High-precision measurement of hydrogen bond lengths in proteins by nuclear magnetic resonance methods. *Proteins*. 35 (3), 275–282. https://doi.org/10.1002/(SICI)1097-0134(19990515)35:3<275::AID-PROT1>3.0.CO;2-V
50. Zheng Y.-Z., Deng G., Zhou Y., Sun H.-Y., & Yu Z.-W. **(2015)** Comparative study of halogen- and hydrogen-bond interactions between benzene derivatives and dimethyl sulfoxide. *ChemPhysChem* 16 (18), 2594–2601. https://doi.org/10.1002/cphc.201500324
51. Anderson C.D., Dudding T., Gordillo R., & Houk K.N. **(2008)** Origin of enantioselection in hetero-Diels–Alder reactions catalyzed by naphthyl-TADDOL. *Org. Lett.* 10(13), 2749–2752.
52. Domingo L.R., & Andrés J. **(2003)** Enhancing reactivity of carbonyl compounds via hydrogen-bond formation. A DFT study of the hetero-Diels–Alder reaction between butadiene derivative and acetone in chloroform. *J. Org. Chem.* 68(22), 8662–8668. https://doi.org/10.1021/jo030156s
53. Polo V., Domingo L.R., & Andrés J. **(2005)** Toward an understanding of the catalytic role of hydrogen-bond donor solvents in the hetero-Diels–Alder reaction between acetone and butadiene derivative. *J. Phys. Chem.* 109(47), 10438–10444. https://doi.org/10.1021/jp054048g
54. Domingo L.R., Asensio A., & Arroyo P. **(2002)** Density functional theory study of the Lewis acid-catalyzed Diels–Alder reaction of nitroalkenes with vinyl ethers using aluminum derivatives. *J. Phys. Org. Chem.* 15(10), 660–666. https://doi.org/10.1002/poc.529
55. Domingo L.R., & Sáez J.A. **(2009)** Understanding the mechanism of polar Diels–Alder reactions. *Org. & Biomol. Chem.* 7(18), 3576–3585. https://doi.org/10.1039/b909611f
56. Alikhani M.E., Fuster F., & Silvi B. **(2005)** What can the topological analysis of ELF tell about hydrogen bonding? *Struct. Chem.* 16(3), 203–210. https://doi.org/10.1007/s11224-005-4451-z

57. Silvi B., & Ratajczak H. **(2016)** Hydrogen bonding and delocalization in the ELF analysis approach. Phys. Chem. *Chem. Phys*. 18(42), 27442–27449. https://doi.org/10.1039/C6CP05400E
58. Fuster F., & Silvi B. **(2000)** Does the topological approach characterize the hydrogen bond? Theor. *Chem. Acc.* 104(1), 13–21. https://doi.org/10.1007/s002149900100
59. Kahn J.O., & Walker B.D. **(1998)** Acute human immunodeficiency virus type 1 infection. *N. Engl. J. Med*. 339(1), 33–39. https://doi.org/10.1056/NEJM199807023390107
60. Gandhi R.T., Bedimo R., Hoy J.F., Landovitz R.J., Smith D.M., Eaton E.F., Lehmann C., Springer S.A., Sax P.E., & Thompson M.A. **(2023)** Antiretroviral drugs for treatment and prevention of HIV infection in adults: 2022 recommendations of the International Antiviral Society–USA Panel. *JAMA* 329(24), 63–84.
61. Saag M.S., Gandhi R.T., Hoy J.F., Landovitz R.J., Thompson M.A., Sax P.E., Smith D.M., Benson C.A., Buchbinder S.P., & Del Rio C. **(2020)** Antiretroviral drugs for treatment and prevention of HIV infection in adults: 2020 recommendations of the International Antiviral Society–USA Panel. *JAMA*. 324(16), 1651–1669.
62. Malik A., Mishra R., Mazumder R., Mazumder A., & Mishra P.S. **(2021)** A comprehensive study on synthesis and biological activities of pyridazine derivatives. *Res. J. Pharm. Technol*. 14(5), 3423–3429. https://doi.org/10.52711/0974-360X.2021.00595
63. Yuan Y.-H., Mao N.-D., Duan J.-L., Zhang H., Garrido C., Lirussi F., Gao Y., Xie T., & Ye X.-Y. **(2023)** Recent progress in discovery of novel AAK1 inhibitors: from pain therapy to potential anti-viral agents. *J. Enzyme Inhib. Med. Chem*. 38(1), 2279906. https://doi.org/10.1080/14756366.2023.2279906
64. Stanzione F., Giangreco I., & Cole J.C. **(2021)** Use of molecular docking computational tools in drug discovery. *Prog. Med. Chem*. 60, 273–343.
65. Parai M.K., Huggins D.J., Cao H., Nalam M.N.L., Ali A., Schiffer C.A., Tidor B., & Rana T.M. (2012) Design, synthesis, and biological and structural evaluations of novel HIV-1 protease inhibitors to combat drug resistance. *J. Med. Chem*. 55(17), 6328–6341. https://doi.org/10.1021/jm300238h
66. Orkideh Ghorban D., Armin Madadkar S., Abbas S., & Massoud M. **(2004)** Flexible ligand docking studies of matrix metalloproteinase inhibitors using Lamarckian genetic algorithm. *DARU J. Pharm. Sci*. 12(1).
67. Razzaghi-Asl N., Sepehri S., Ebadi A., Miri R., & Shahabipour S. **(2015)** Effect of biomolecular conformation on docking simulation: a case study on a potent HIV-1 protease inhibitor. *Iran. J. Pharm. Res*. 14(3), 785–802. PMID: 26330867.
68. Cuozzo A., Daina A., Perez M.A., Michielin O., & Zoete V. **(2022)** SwissBioisostere 2021: Updated structural, bioactivity and physicochemical data delivered by a reshaped web interface. *Nucleic Acids Res*. 50(D1), D1382–D1390. https://doi.org/10.1093/nar/gkab1047
69. Dahlgren D., & Lennernäs H. **(2019**) Intestinal permeability and drug absorption: predictive experimental, computational and in vivo approaches. *Pharmaceutics* 11(8), 411. https://doi.org/10.3390/pharmaceutics11080411
70. Ojuka P., Kimani N.M., Apollo S., Nyariki J., Ramos R.S., & Santos C.B. **(2023)** Phytochemistry of plants in the genus Vepris: A review and in silico analysis of their ADMET properties. *S. Afr. J. Bot*. 157, 106–114. https://doi.org/10.1016/j.sajb.2023.03.057
71. Rasgania J., Gavadia R., & Jakhar K. (2023) Facile synthesis, pharmacological and in silico analysis of succinimide derivatives: an approach towards drug discovery. *J. Mol. Struct*. 1274, 134424. https://doi.org/10.1016/j.molstruc.2022.134424
72. Supandi S., Wulandari M.S., Samsul E., Azminah A., Purwoko R.Y., Herman H., Kuncoro H., Ibrahim A., Ambarwati N.S.S., & Rosmalena R. **(2022)** Dipeptidyl peptidase IV inhibition of phytocompounds from Artocarpus champeden (Lour.) Stokes: in silico molecular docking study and ADME-Tox prediction approach. *J. Adv. Pharm. Technol. Res.* 13, 207. https://doi.org/10.4103/japtr.japtr_376_22
73. Salekeen R., Siam M.H.B., Sharif D.I., Lustgarten M.S., Billah M.M., & Islam K.M.D. **(2021)** In silico insights into potential gut microbial modulation of NAD^+ metabolism and longevity. *J. Biochem. Mol. Toxicol*. 35(1), e22925. https://doi.org/10.1002/jbt.22925.
74. Zoubir M., Belghiti M.E., El idrissi M., & Zeroual A. **(2022)** Theoretical investigation of the mechanism and regioselectivity of the 3-isopropyl-1, 6-dimethyl-naphthalene and ar-himachalene in nitration reaction: a MEDT study. *Theoretical Chemistry Accounts*, 141(2), 8. https://doi.org/10.1007/s00214-022-02869-7

© 2026 by the authors; licensee Growing Science, Canada. This is an open access article distributed under the terms and conditions of the Creative Commons Attribution (CC-BY) license (http://creativecommons.org/licenses/by/4.0/).